

Article

# Experimental Measurement Method for Contact Stress of Elastic Metal Sealing Ring Based on Pressure Sensitive Paper

Miaotian Zhang <sup>1,\*</sup> , Shuangfu Suo <sup>2</sup>, Yang Jiang <sup>2</sup> and Guoying Meng <sup>1</sup>

<sup>1</sup> School of Mechanical Electronic & Information Engineering, China University of Mining and Technology Beijing, Beijing 100083, China; mgy@cumtb.edu.cn

<sup>2</sup> School of Mechanical Engineering, Tsinghua University, Beijing 100084, China; sfsuo@mail.tsinghua.edu.cn (S.S.); y-jiang15@mail.tsinghua.edu.cn (Y.J.)

\* Correspondence: zhangmiaotian1231@163.com; Tel.: +86-186-0080-3106

Received: 31 August 2018; Accepted: 11 November 2018; Published: 13 November 2018



**Abstract:** As a basic mechanical component, the sealing ring is widely used in industrial, aerospace, and other fields. In this study, an elastic metal C-shaped sealing ring with a wave structure was taken as an example, and its performance was analyzed theoretically and measured experimentally. First, an experimental study was performed on the C-ring seal. The proposed method for experimental measurement of the contact stress of the C-ring seal involved innovative use of a universal electronic testing machine and pressure sensitive paper, in conjunction with the hue–saturation–brightness (HSB) method. Based on the discoloration of the pressure sensitive paper after contact stress, computer software was used for analysis, the discoloration was digitized, and the contact stress was established. Second, a theoretical calculation model of the C-ring seal was established using ANSYS software, and a finite element theoretical calculation of the mechanical properties of the sealing ring was established. Finally, the contact stress results were compared with the model calculation results of the C-ring seal. The error between the two was small (4.8%), which proved the validity of the calculation model and the scientificity of the experimental method.

**Keywords:** C-shaped elastic metal sealing ring; contact stress measurement; pressure sensitive test paper; HSB method; finite element analysis

## 1. Introduction

Seals are key infrastructure components in many high-tech fields, including the aerospace and ergonomics industries [1,2]. In conjunction with industrial development, elastic metal sealing technology has also developed rapidly. In the field of aerospace engines, seals are constantly subjected to severe working conditions that include high temperatures, high pressures, and strong vibrations. It is difficult for conventional seals to exhibit good performance under such severe conditions, and leakage could occur through a gap that might appear between a seal and a flange after exposure to a continuously alternating load. A corrugated elastic metal ring has a unique structure and with its opening facing the high-pressure side, self-tightening can be achieved because of the pressure of the sealing medium. Common wave seals include both C- and W-shaped seals. When a C-shaped sealing ring is in operation, its opening tends to face the high pressure of the sealing gas, which means C-ring seals have excellent self-tightening capability. Moreover, under a cyclic alternating load, the pressure of the sealing gas can help a C-ring seal rebound, which can help block any gap between the sealing ring and the flange, preventing leakage [3].

Many previous studies have undertaken considerable research on C-ring seals. In terms of performance research, Polycarpou [4] studied the contact width law of a C-ring and flange,

and calculated the leakage of a C-ring seal using the GW model. Lefrançois et al. [5] used CAE calculation software to simulate the sealing performance of C-ring seals. In experimental research, Blanton et al. [6] conducted a leak test of a spring-plated silver C-ring seal to elucidate the effects of operating temperature, medium pressure, flange eccentricity, torque, surface roughness, penetration, and reuse on the amount of leakage. Xiong Guangming et al. [7] established a C-shaped sealing ring model to simulate the process of loading and unloading. Jia Xiaohong et al. [8] established a 3-dimensional simulation model of a spring-enhanced C-shaped sealing ring, and they performed an in-depth study on the compression and rebound characteristics of the sealing ring. Dong Yuanyuan et al. [9] established a 3-dimensional finite element model of a C-shaped seal to analyze its sealing and compression–rebound characteristics, and they performed compression–rebound experiments.

Research on elastic metal seals is reasonably mature. Because of the excellent performance of elastic metal seals, in addition to the aerospace field, the technology has also been used widely in the nuclear, chemical, and pharmaceutical industries [10]. The world-famous sealing company headed by JETSEAL has applied for a number of technical patents and it has commercialized various types of elastic metal sealing ring with various cross-sectional shapes. The current research status of C-shaped elastic metal seals is based largely on performance research [8,11]. However, in the experimental study of C-ring seals, although techniques for the determination of compression–rebound characteristics are well established, there is no mature experimental method for testing contact stress.

This study used a universal electronic testing machine to pressurize a C-ring seal. The contact pressure of the C-ring was measured using the hue-saturation-brightness (HSB) method by a pad under the C-ring. The finite element analysis results were found to be highly consistent with experimental measurements, validating the feasibility and scientificity of the proposed experimental method.

## 2. Working Principle of Sealing Ring

Elastomeric metal seals are generally installed between upper and lower flanges. The structure of a sealing ring, for which the principal failure mode is leakage, is shown in Figure 1. There are two basic conditions for leakage: Pressure difference between the inside and outside of the sealing ring, and a small leakage channel between the surface of the seal and the flange surface [12]. In an elastic metal-sealed working environment, pressure difference between the inside and outside of a sealing ring is unavoidable; therefore, minimizing leakage channels is the only way to reduce or prevent leakage.

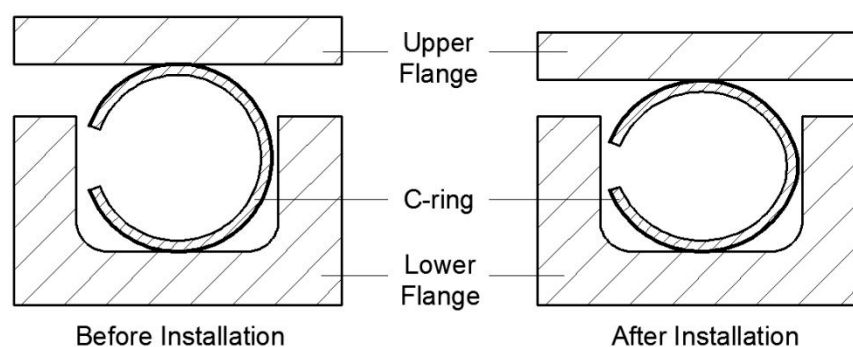
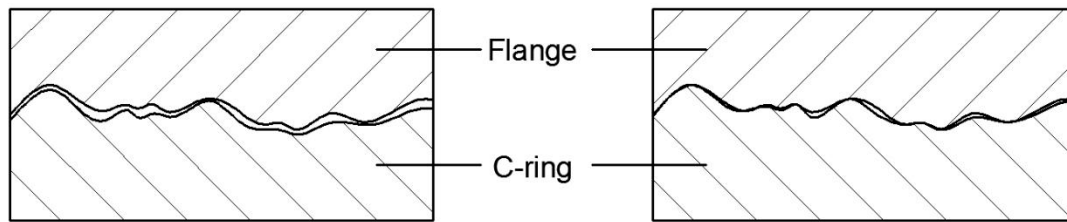


Figure 1. Schematics of C-shaped metal sealing ring structure.

Figure 2 shows a schematic of the microscopic principle of a C-ring seal [13]. The picture on the left represents a microscopic view of the surfaces of the seal and the flange in contact but without a preload. At this time, although the surface of the sealing ring is in macroscopic contact with the flange, a microscopic leakage channel exists because of surface roughness; thus, the sealing ring cannot fulfill the function of preventing leakage. The picture on the right is a schematic representation of the microscopic surfaces after the application of a preload to the flange. At this time, because of the

preloading force, the metal plating on the surface of the sealing ring is extended and in full contact with the flange, filling the leakage channel and thereby preventing leakage.



**Figure 2.** Schematics of microscopic leakage channel.

The metal plating on the surface of a C-ring seal is fundamental in ensuring sealing performance. Because the surface ductile soft metal coating of a C-ring seal is subjected to pressure, it can fully fill the microscopic leakage channels between two surfaces, such that sealing performance can be guaranteed.

### 3. C-Ring Contact Stress Measurement Method

One of the most important factors affecting the performance of seal is the maximum contact pressure at which the seal operates. According to the actual working conditions of C-ring, a simulation experiment was carried out to measure the maximum contact pressure. The experimental temperature was 16 °C and the correlative humidity was 23%.

#### 3.1. Experimental Device

##### 3.1.1. Measurement Samples

The metal C-ring seal sample (Figure 3) used for the measurement experiments was purchased from a company in Shanghai.



**Figure 3.** Measurement sample.

##### 3.1.2. Contact Stress Measuring Device

In the experiment, Fujifilm pressure sensitive paper was used for measuring the contact stress. According to the simulation results of the C-ring seal, the HSB model was selected for the experimental pressure sensitive paper.

The principle of measuring contact pressure using pressure sensitive paper is as follows.

Figure 4 presents a schematic of the microstructure of the pressure sensitive paper used in the experiments. The pressure sensitive paper has a three-layer structure comprising a polyester base layer, a thin color-development layer, and a thin microencapsulated color-forming layer. This structure reveals different colors under different pressures.

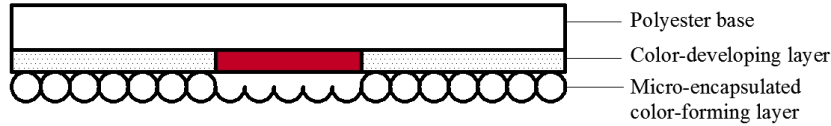


Figure 4. Structure of pressure sensitive paper.

Figure 5a shows the color-contact pressure reference curve given in the pressure sensitive paper specification. As shown in the Figure 5b, curve A or curve B is selected according to the correlative humidity and temperature at the time of measurement. The correlative humidity in this experiment was 23% and the temperature was 16 °C, so curve B was selected. When the pressure sensitive paper is discolored under a certain contact pressure, it is compared with the standard color card, and its color coefficient is selected; thus, the contact pressure value is read in the corresponding graph. However, certain error is inherent in this reading method, i.e., reading of the color is a subjective judgment, which means the requirements of high-precision testing cannot be satisfied. Therefore, in the experiments of this study, image analysis software was used to digitize the color card, and the digitized color index and contact stress were fitted correspondingly to obtain an accurate contrast curve.

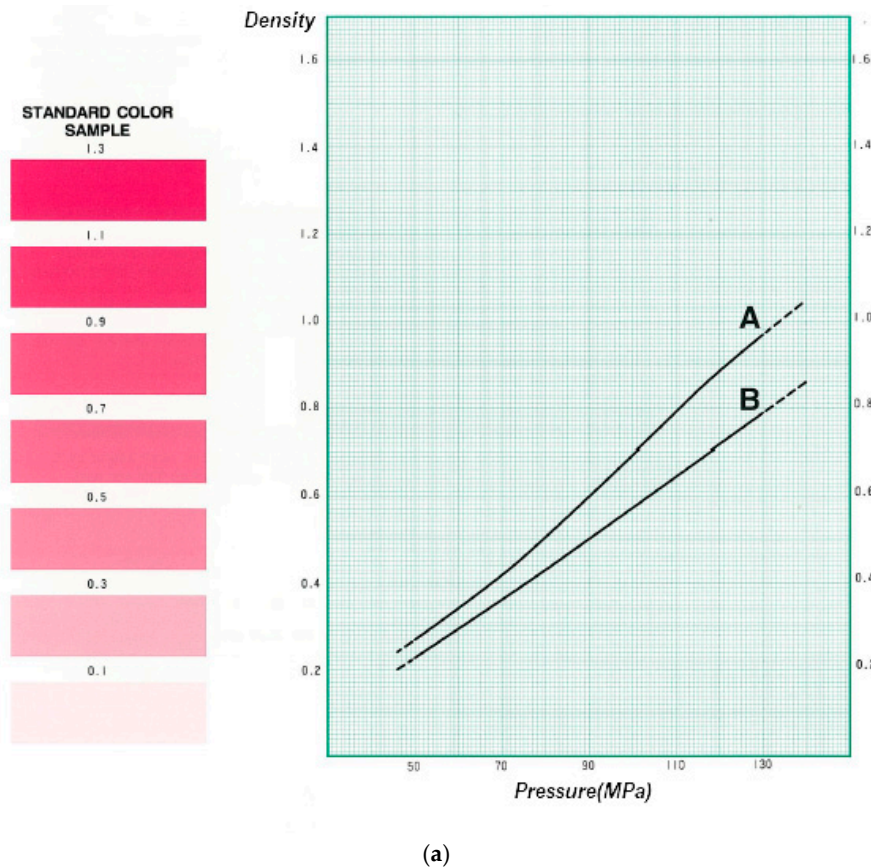


Figure 5. Cont.

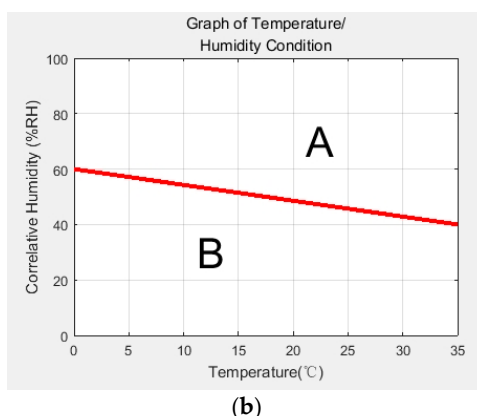


Figure 5. (a) Color-contact pressure scan of pressure sensitive paper; (b) Curve selection criteria.

A color model is a mathematical model that uses a set of values to describe a color. Color models used commonly in color image processing include the red-green-blue (RGB), hue-saturation-intensity, and HSB models. The traditional RGB model is the model used most commonly for three primary colors. The HSB method (also known as the HSV method) uses hue, saturation, and brightness to define a color. In this case, hue refers to the type of color, saturation refers to the change in purity of a color (i.e., the degree to which a color changes between absolute gray and absolute color), and brightness is a measure of the brightness of a color. The higher the B value, the brighter the color, and the closer it is to white. Conversely, the lower the B value, the darker the color, and the closer it is to black. Compared with the RGB space, the HSB space can express with high precision and accuracy the brightness, color, and vividness of a color very intuitively, which is convenient for contrast between colors. Compared with the RGB processing method, the HSB method is more attuned to human cognition of color. In contrast, the RGB method is a color-friendly method that is suitable for machine processing; however, the RGB and HSB spaces can be mutually transformed [14].

Use Photoshop software to color-code the color card, and use the HSB method to color-code the color card.

The color card in the manual was analyzed using the HSB method, and the corresponding relationship obtained is shown in Table 1.

Table 1. Correspondence between color cards.

Color Coefficient	H	S	B
1.3	339	87	90
1.1	340	75	89
0.9	343	60	90
0.7	342	51	91
0.5	343	40	91
0.3	346	23	92

It can be seen from Table 1 that as the color coefficient changes, the change of the S value is particularly obvious, while the H and B values do not change substantially. Therefore, the S value was chosen as the calibration factor for the color in this experiment.

### 3.1.3. Compression Force Applying Device

The device used for the application of compression in the experimental tests was a universal electronic testing machine (WDW-100/E) at the Key Laboratory of Applied Mechanics of Tsinghua University (Beijing, China). This test machine can perform compression, stretching, and bending experiments under large loads and at various temperatures. The test machine is controlled by a computer equipped with software, that can derive compression-rebound measurement data,

and provide real-time monitoring of compression force and displacement. The experimental setup is shown in Figure 6.

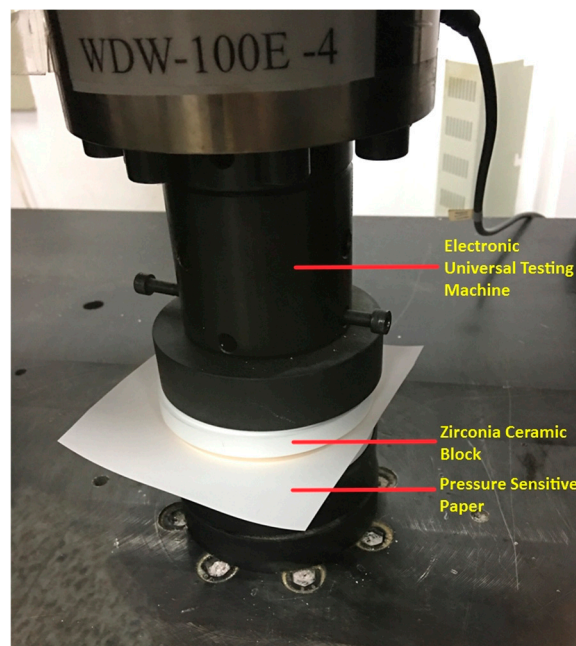


**Figure 6.** Experimental device.

#### 3.1.4. Auxiliary Gasket Device

Contact stress, one of the measurement objects of this experiment, is affected considerably by flatness. However, the compression platform of the universal electronic testing machine is not completely flat. Therefore, a pressure-resistant zirconia ceramic block was used as an experimental gasket, and a concentric pad was placed between the upper pressing head and the lower platform. During the experiment, the pressure sensitive paper and the sealing ring were placed between two zirconia ceramic sheets, such that the sealing ring could be pressed under a completely flat state.

Zirconia has the characteristics of a high melting point, a high boiling point, and high hardness level. The compressive strength of the zirconia ceramic sheets used in this study was up to 1200 MPa. As the maximum compressive strength of the experiments was estimated at 800 MPa, the safety factor of the device was 1.5.

#### 3.2. Experimental Operation and Parameters

The test bench was calibrated first. This confirmed the correct operation of the universal electronic testing machine, LCD screen, and computer and it verified that the control system operated the indenter correctly.

The pressure sensitive paper was cut according to the experimental specifications and placed between two zirconia ceramic sheets. The zirconia ceramic sheets were located between the upper and lower indenters to maintain concentric alignment to ensure uniform application of force. The indenter was moved to a location close to but not in contact with the upper tile. When the speed was selected as 0.2 mm/min, the control head moved downward automatically until it could be observed by the computer that the force sensor was not zero. After the force sensor first produced a number, the compression rebound experiment module was selected on the computer; the pressing speed was selected as 0.02 mm/min, and the compression was suspended when the compression reached 0.24 mm. When the maximum compression amount was reached, the pressure was maintained for 2 min, and the pressure sensitive paper was fully subjected to pressure discoloration.

To move the head upward, the direction of head displacement was changed and a speed of 0.4 mm/min was selected. When the indenter returned to the origin of its displacement, the compression rebound experimental data were saved. The pressure sensitive paper was then scanned together with the color card for analysis of the experimental data.

The experimental parameters are shown in Table 2.

**Table 2.** Experimental parameters.

Parameter Name	Parameter Value
Seal outer diameter (mm)	40.6
Seal free height (mm)	2.39
Wall thickness (mm)	0.25
Coating thickness (mm)	0.03
Experimental temperature (°C)	20
Medium pressure (MPa)	0
Compression amount (mm)	0.24
Compression speed (mm/min)	0.02
Unloading speed (mm/min)	0.04

### 3.3. Experimental Results and Analysis

According to the above experimental steps and operations, contact stress measurements were performed on the C-ring seal, which produced results as shown in Figure 7.

The pressure sensitive paper was scanned in the same file as the color card to avoid interference with the color analysis results of the scanning device. As described above, the color card and indentation were interpreted using the HSB color model, after the scanned color card was analyzed, as shown in Figure 8.

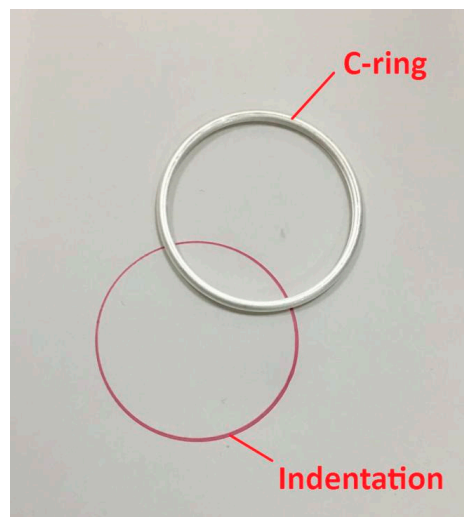


**Figure 7.** Photo of experiment result.



**Figure 8.** Contact experiment color card scan.

Using the Photoshop software color picking function, multiple points were acquired randomly in the pixels of each color card, and their S values were read and recorded. The averages of these values were taken as the final S value for each color card. The specific results are shown in Table 3.

**Table 3.** Color card S value calibration.

Color Card Coefficient	Color Coefficient
1.3	75.63
1.1	71.12
0.9	64.22
0.7	52.74
0.5	42.23
0.3	24.12
0.1	6.89

According to Table 3, the calibration S value was matched with the color card coefficient using the linear fitting method. The specific results are shown in Formulas (1)–(6):

$$y = (x - 71.12) \times 0.044346 + 1.1 (71.12 \leq x < 75.63) \quad (1)$$

$$y = (x - 64.22) \times 0.028986 + 0.9 (64.22 \leq x < 71.12) \quad (2)$$

$$y = (x - 52.74) \times 0.017422 + 0.7 (52.74 \leq x < 64.22) \quad (3)$$

$$y = (x - 42.23) \times 0.019029 + 0.5 (42.23 \leq x < 52.74) \quad (4)$$

$$y = (x - 24.12) \times 0.011044 + 0.3 (24.12 \leq x < 42.23) \quad (5)$$

$$y = (x - 6.89) \times 0.011608 + 0.1 (6.89 \leq x < 24.12) \quad (6)$$

At this point, the work of establishing the correspondence between the color change of the indentation and the color card value has been completed. The establishment of this correspondence makes it possible to avoid subjectivity and experimental errors attributable to color recognition by the human eye in the processing of the experimental results. In the processing of the experimental results, multiple points can be collected by the computer software to identify accurately the color change of

the experimental results. Then, using the relationship between the color coefficient and the contact stress given in the specification of the pressure sensitive paper, the contact stress value associated with the color change derived from the experimental results can be obtained.

Figure 9 shows an enlarged view of the experimental indentation scan. By finding the deepest indentation and the darkest part of the experimental results, the computer software was used to obtain the S values of random multiple color-changed pixels. In this example, the average S value of this indentation was 70.22. Using the correspondence between the S value and the color card coefficient in Formulas (1)–(6), the color card coefficient corresponding to the indentation was determined as 1.07. Using the corresponding relationship between the color card coefficient and the contact stress (Figure 5), the contact stress of the indentation of this section was established as 140 MPa.

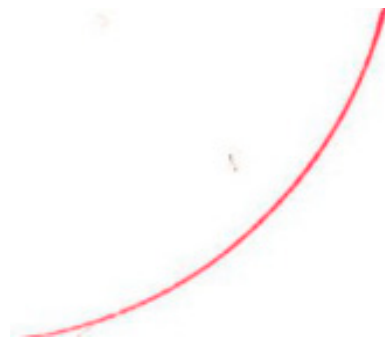


**Figure 9.** Enlargement of experimental indentation scan.

#### **4. Finite Element Analysis of C-Ring Seal**

##### *4.1. Model Establishment*

The calculation model of a C-ring seal was established using ANSYS numerical simulation software. Because the cross-sectional shape of a C-ring seal is consistent, a 2-D rotational symmetry model was selected for the calculation. Figure 10 shows the finite element simulation flow chart.

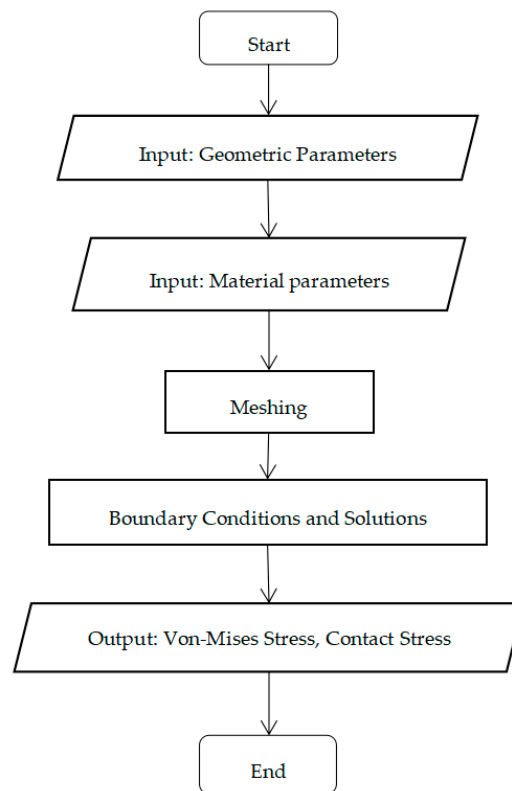


**Figure 10.** Finite element simulation flowchart.

#### 4.1.1. Geometric Model

According to the 1 purchased by a company in Shanghai (China), a finite element model is established. The structural geometric parameters of the C-ring seal are shown in Table 4.

**Table 4.** Geometric parameters of the C-ring seal.

Geometric Parameter	Value (mm)
Seal outer diameter	40.6
Seal free height	2.39
Elastic metal wall thickness	0.25
Plating metal thickness	0.03

In the calculation of the finite element model of the C-ring, the entire section and the upper and lower flanges were selected as the modeling objects. In the selection of the calculation unit, the Plane 182 unit was selected as the calculation unit of the C-ring seal. In considering the calculation of contact stress, Contact 172 and Target 169 were selected as a contact pair, where Contact 172 and Target 169 represent the C-ring seal plating and the upper and lower flange contact faces.

#### 4.1.2. Material Model

A bilinear isotropic strengthening material constitutive model was selected that adopted Inconel 718 as the alloy body material and silver as the plating material (Table 5).

**Table 5.** ANSYS modeling material parameters of C-ring [15,16].

Material	Elastic Modulus/GPa	Poisson's Ratio	Yield Strength/MPa	Plastic Section Slope/GPa
Inconel 718	214	0.3	1150	4
Silver	82	0.38	30	0.418

#### 4.1.3. Meshing

Meshing was undertaken in accordance with the structure of the C-ring seal.

#### 4.1.4. Boundary Conditions and Solutions

In accordance with the actual working conditions, the calculation is divided into two steps:

- (1) Set up the geometric model of the C-ring seal, complete the unit selection, material model construction, and mesh division. At this time, the C-ring is in a critical state of contact with the flange, which is also an initial state.
- (2) Displacement is applied to the upper flange to cause a predetermined amount of compression (0.24 mm). At this time, a force acts between the C-ring seal and the flange, causing deformation. In this state, the von Mises stress distribution and contact stress distribution of the C-ring are read as the calculation results of the mechanical properties under the working conditions, as shown in Figure 11.

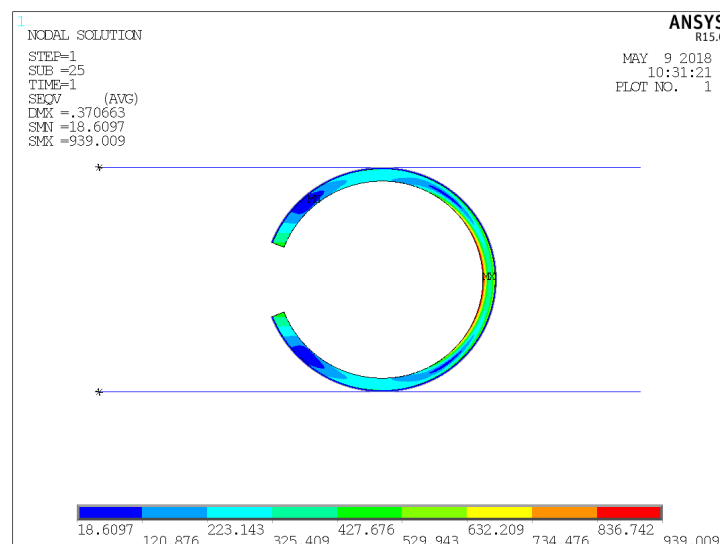


**Figure 11.** Von Mises stress distribution of the C-ring seal.

## 4.2. Analysis of Calculation Results

### 4.2.1. Von Mises Stress Distribution

As can be seen from Figure 1, the area of concentration of von Mises stress in the C-ring seal in the working state is on the closed-side rib. Therefore, to alleviate the stress concentration on the closed-side rib, local reinforcement could be performed for the rib force or the left-side opening portion could be designed as a pressure-bearing structure with reference to the special C-shaped design.

Under the imposed working conditions, the maximum von Mises stress of the C-ring is 939.009 MPa, which does not exceed the yield strength of Inconel 718 (1150 MPa; refer to Table 2). Therefore, the stability of the C-ring seal is considered adequate under the imposed working conditions.

### 4.2.2. Contact Stress Distribution and Analysis

Figure 12 shows the contact stress distribution of the contact surface of the C-ring seal under the imposed working conditions.

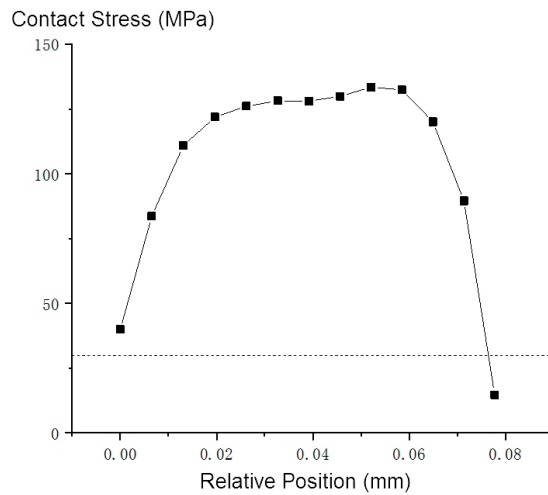


Figure 12. Contact stress distribution of the C-ring seal.

It can be seen from the figure that the contact stress distribution exhibits rapid rise and fall separated by a zone of stability. The auxiliary line in Figure 4 is the yield strength of the silver layer. It is clear that the contact stress corresponding to most of the contact width is above the yield strength of the silver layer, which allows the silver layer to become fully deformed and to extend to fill the leakage channels between the surfaces of the seal and the flange.

The finite element calculation was performed using the C-ring seal model, and the obtained contact stress distribution results are shown in Figure 13. The maximum contact stress was 133.57 MPa, which is very close to the experimentally measured value of 140 MPa, i.e., the error between them is only 4.8%. This not only proves the validity of the theoretical model but it also confirms the scientificity of the proposed experimental method.

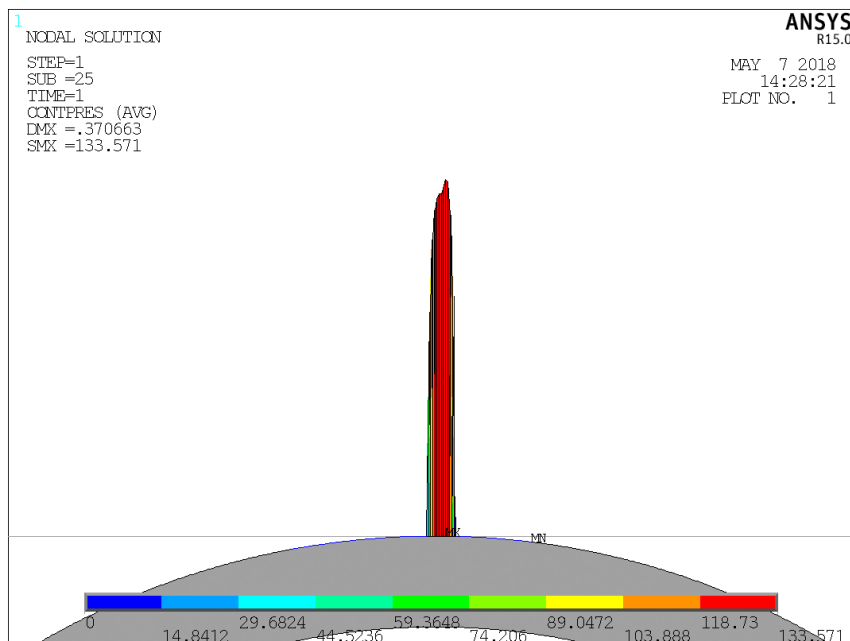


Figure 13. Model stress calculation results.

### 5. Conclusions

In this study, the contact stress of a C-ring seal was measured through innovative application of a universal electronic testing machine and pressure sensitive paper. Moreover, finite element modeling

and analysis of an elastic metal C-ring seal was performed using ANSYS software. The principal conclusions derived are as follows:

- (1) The contact stress of the elastic metal C-ring seal was measured using an innovative application of a universal electronic testing machine and pressure sensitive paper. A finite element analysis was undertaken prior to performing the experiments. According to different pressure ranges, contact strip width, and other factors, different pressure sensitive papers were selected and the experimental scheme was developed to measure the contact stress. However, the proposed method is unsuitable if the contact width is too narrow.
- (2) Compared with the traditional RGB method, the HSB color model obtains measurement results that are more accurate. The discoloration of the pressure sensitive paper was calibrated using the HSB color model, and the experimental results were processed using computer software to obtain accurate measurement of the maximum contact stress value of the C-ring seal.
- (3) The area of concentration of von Mises stress of the C-ring seal in its working state was found on the closed-side rib, and the maximum von Mises stress was 939.009 MPa. The contact stress distribution was found to exhibit rapid rise and fall separated by a zone of stability. Therefore, it was considered that the stability of the C-ring seal was adequate under this condition.
- (4) The experimental measurement results were found in satisfactory agreement with the calculation results of the finite element modeling, i.e., the error was only 4.8%. This not only proves the validity of the theoretical model but it also confirms the feasibility and scientificity of the experimental method. This study proposed a new, simple, and easy to use experimental method for measuring the contact stress of elastic metal seals that could be used as the basis for positive seal design. This experimental method could also be used to measure the contact pressure of other metals.

In the future, we will focus on extending this method to a variety of elastic metal sealing rings, and truly form a system of contact stress measurement methods, laying the foundation for the industrial development of elastic metal seals.

**Author Contributions:** Conceptualization, M.Z. and S.S.; methodology, M.Z.; software, Y.J.; validation, M.Z., S.S. and G.M.; formal analysis, M.Z. and Y.J.; investigation, M.Z.; resources, S.S.; data curation, G.M.; writing—original draft preparation, M.Z.; writing—review and editing, M.Z. and S.S.; visualization, S.S.; supervision, G.M.; project administration, S.S.; funding acquisition, S.S.

**Funding:** This research was funded by National Program on Key Basic Research Project, the grant number is 2014CB046404.

**Conflicts of Interest:** The authors declare no conflict of interest. The funders had no role in the design of the study; in the collection, analyses, or interpretation of data; in the writing of the manuscript, or in the decision to publish the results.

## References

1. Craggs, A. The transient response of a couple plate-acoustic system using plate and acoustic finite elements. *J. Sound Vib.* **1971**, *4*, 509–528. [[CrossRef](#)]
2. Suzuki, S. Boundary element analysis of cavity noise problems with complicated boundary. *J. Sound Vib.* **1989**, *130*, 147–153. [[CrossRef](#)]
3. Xing, M.J. Study on Sealing Performance and Leakage of Metal W-ring in the Aircraft Engine. Master's Thesis, Beijing Institute of Technology, Beijing, China, 2015.
4. Polycarpou, A.A.; Etsion, I. A model for the static sealing performance of compliant metallic gas seals including surface roughness and rarefaction effects. *Tribol. Trans.* **2000**, *43*, 237–244. [[CrossRef](#)]
5. Lefrançois, M.; Montuclard, J.; Rouaud, C. Low-load metal seals to replace elastomer O-rings: The Helicoflex-delta ( $\Delta$ ) seals. *Vacuum* **1990**, *41*, 1879–1881. [[CrossRef](#)]
6. Blanton, P.S.; Eberl, K.R. Performance testing of spring energized C-Rings for use in radioactive material packagings containing tritium. In Proceedings of the 15th International Symposium on the Packaging Transportation of Radioactive Materials PATRAM, Miami, FL, USA, 21–26 October 2007; pp. 21–26.

7. Xiong, G.M.; Duan, Y.G.; Deng, X.Y.; Tan, W.; Jin, T.; Yang, N.R. Numerical simulation research on C-ring of CPR1000 reactor pressure vessel. *Nucl. Power Eng.* **2012**, *33*, 9–12.
8. Jia, X.; Chen, H.; Li, X.; Song, W. Analysis on the mechanical and sealing properties of metallic C Ring. *Lubr. Eng.* **2014**, *39*, 1–5.
9. Dong, Y.; Luo, Y.; Zhang, L.; Li, P. Study on numerical Simulation for sealing behavior of C-Ring. *Nucl. Power Eng.* **2015**, *36*, 155–159.
10. Zhang, W.L. Elastic Metal Seal Technology. *Hydraul. Pneum. Seals.* **2009**, *3*, 4–7.
11. Wenjing, L.I.; Shen, M.; Peng, X.; Xinggen, L.I.; Zheng, J.; Wang, Y. Effect of spring structure parameters on mechanical behavior and sealing performance of spring energized metal C-Ring. *Lubr. Eng.* **2016**, *41*, 71–77.
12. Cui, X.J. Research progress and sealing mechanism analysis of metal sealing technology. *Chin. Petrol. Mach.* **2011**, *39*, 102–105.
13. Feng, X. *Metal Gasket Sealing Model and Application Research*; Nanjing Tech University: Nanjing, Chian, 2006.
14. Wu, L.L. Conversion expression of RGB color model to HSB color model. *Mod. Mach.* **2007**, *3*, 28–29.
15. Yin, S. *Welding Materials Handbook*, 3rd ed.; China Standard Press: Beijing, China, 2000; ISBN 9787506655613.
16. Li, Q.Q. Structure Simulation and Optimization of Sealing Performance of Metal C-ring with Built-in Spring. Master's Thesis, Beijing University of Chemical Technology, Beijing, China, 2017.



© 2018 by the authors. Licensee MDPI, Basel, Switzerland. This article is an open access article distributed under the terms and conditions of the Creative Commons Attribution (CC BY) license (<http://creativecommons.org/licenses/by/4.0/>).